DEVELOPMENT OF TiO_2-REDUCED GRAPHENE OXIDE NANOCOMPOSITES AND THEIR ENHANCED PHOTOCATALYTIC AND PHOTOVOLTAIC PERFORMANCE

D. XU*, P. WANG, B. SHEN
College of Geomatics and Municipal Engineering, Zhejiang University of Water Resources and Electric Power, Hangzhou 310018, P.R. China

In this contribution, TiO_2–reduced graphene oxide (RGO) nanocomposites were synthesized via an ultrasonication-assisted reduction method using graphene oxide (GO) in the TiO_2 precursor solution. The reduction of GO and the formation of TiO_2 crystals occurred simultaneously. The synthesized nanocomposite was characterized by SEM, EDX, Raman spectroscopy, FTIR, XRD, XPS, UV-vis spectroscopy, photoluminescence spectrometer and electrochemical impedance spectroscopy. As a result of the introduction of RGO, the light absorption of octahedral TiO_2 was markedly improved. The results revealed that weight percent of RGO has substantial influence on degradation of Rhodamine B under visible light irradiation. The enhancement of the photocatalytic activity was attributed to more harvesting of the visible-light irradiation and efficiently separation of the photogenerated charge carriers. Meanwhile, upon the RGO loading, the photoelectric conversion efficiency of TiO_2-RGO nanocomposite modified electrode was highly improved

(Received November 4, 2015; Accepted January 6, 2016)

Keyword: TiO_2; Reduced graphene oxide; Nanocomposite; Photocatalyst; Photovoltaic activity

1. Introduction

Titanium dioxide is an important n-type semiconductor with a band gap of 3.2 eV, has been extensively used in photocatalytic degradation of organic pollutants, hydrogen production, antibacterial materials and solar cells because of its high efficiency, low cost, chemical inertness, and high photo-stability [1-5]. However, TiO_2 suffers from the limited absorption of solar light as a result of its large band gap and low quantum yield because of the fast recombination of photo-generated charges. In this context, typical photocatalysts have been modified in order to enhance their solar photocatalytic activity, by doping, metal particle deposition or even by their combination with other materials to produce highly photoactive composites [6-8].

Among different materials that can be selected to prepare composites with TiO_2, carbon materials offer unique advantages, such as chemical inertness and stability, in both acid and basic media, and tunable textural and chemical properties [9-13]. Graphene, a two-dimensional, single-layer sheet of carbon atoms that are closely packed into a hexagonal lattice structure, is a very promising candidate for high performance photocatalyst because of its excellent thermal conductivity, excellent mobility of charge carriers and large specific surface area [14-20]. The first work found in the literature about the preparation of RGO–TiO_2 composites by UV-assisted photocatalytic reduction was presented by Williams et al.[21] They observed how GO was reduced due to the acceptance of generated electrons from UV-irradiated TiO_2 suspensions, and proposed a graphene–semiconductor mechanism. Following that, many research groups carried out one-step hydrothermal methods to prepare graphene-TiO_2 hybrid materials and showed that the composites exhibited enhanced photoactivity towards organic degradation over bare TiO_2. Fan et al.[22]

*Corresponding author: xud@zjweu.edu.cn

reported the fabrication of P25-graphene composites by, UV-assisted photocatalytic reduction, hydrazine reduction and hydrothermal method. However, only small number of reports regard the synthesis of graphene-TiO_2 nanocomposite by ultrasonication method. Therefore, in this work, a TiO_2–RGO nanocomposite has been successfully prepared via a simple ultrasonication approach. In order to inspect the effect of RGO, the properties of as-synthesized nanocomposites were evaluated by a series techniques. Moreover, the effect of GO ratio in the preparation stage also been studied. In addition, the photocatalytic and photovoltaic performances of TiO_2–RGO nanocomposite were evaluated and compared with those of pure TiO_2.

2. Experimental

2.1 Materials

GO was synthesized by the modified Hummers method using natural graphite as precursor [23]. Briefly, 2 g of graphite powder and 1.25 g $NaNO_3$ were added to 60 mL of concentrated H_2SO_4. 7.5 g of $KMnO_4$ was added gradually with stirring and cooling to maintain the mixture below 20 °C. The mixture then stirred at 35 °C for 30 min. 120 mL of distilled water was slowly added to the mixture and the temperature increased to 98 °C, then the mixture was maintained at this temperature for 15 min. The reaction was terminated by adding 350 mL of distilled water followed by 10 mL of 30% H_2O_2 solution. The solid product was separated by centrifugation, washed repeatedly with 5% HCl solution until sulfate could not be detected with $BaCl_2$, and then washed three times with ethanol and dried in vacuum at 60 °C overnight. $C_{16}H_{36}O_4Ti$ (TNB), 1-butyl-3-methylimidazolium iodide (BMIMI), tert-butylpyridine, LiI, acetonitrile, valeronitrile and Rhodamine B (Rh B) were were purchased from Sigma-Aldrich. All other chemicals used were analytical grade reagents without further purification

2.2 Preparation of TiO_2–reduced graphene oxide nanocomposite

In a typical synthesis of TiO_2-RGO nanocomposite, TNB precursors were fabricated by preparing a solution with a molar ratio of ethanol: H_2O:TNB of 35:15:4. GO (0.2 g) was added and the resulting mixture was stirred for 0.5 h at ambient temperature. 100 mL 1 M NaOH was then added into the above solution. After ultrasonication for 15 min, 1.5 mL NH_2OH•HCl was added into the blue solution. The reaction mixture was then treated with high-intensity ultrasound (100 W, 40 kHz) at room temperature in air for a certain period of time. The products were filtered, washed repeatedly with distilled water and ethanol, and then vacuum dried at 60 °C. The dried catalyst was ground in a ball mill and calcined at 150 °C for 3 h to obtain a TiO_2-RGO nanocomposite. For comparison, TiO_2 nanoparticles were prepared by a similar process without adding GO. The reduction of GO was also achieved from the same method without adding TNB.

2.3 Characterization

The surface morphology of the samples was analyzed by a field emission scanning electron microscope (FESEM, ZEISS SUPRA 40VP). Raman spectroscopy was performed at room temperature using a Raman microscope (Renishaw, inVia) with 514 nm laser light. The surface functional groups present on the samples were analyzed by Fourier transform infrared spectroscopy (FTIR, Nicolet iS5, Thermo Scientific, USA). X-ray photoelectron spectroscopy (XPS) measurements were performed in a VG Multilab2000 spectrometer to obtain the information on chemical binding energy of the samples. X-ray diffraction (XRD) patterns were carried out using X'Pert Philips diffractometer with Cu anode. Photoluminescence (PL) spectra were measured at room temperature on a fluorescence spectrophotometer (F-7000, Hitachi, Japan). The excitation wavelength was 315 nm. The optical properties of the samples were analyzed by UV-vis diffuse reflectance spectroscopy (UV-vis DRS) using a UV-vis spectrophotometer (Cary-500, Varian Co.)

2.4 Photoelectrochemical measurement

As-prepared nanocomposites were deposited onto a fluorine-doped tin oxide (FTO) by spin coating method, which used as a photoanodes in solar cells. The solar cells were fabricated in

a sandwich approach by placing a platinum coated conducting glass on the dye-sensitized photoanode. The active area of the solar cell was 6×6 mm^2. The photochemical performances of samples were investigated using a standard three-electrode system, with a coiled Pt wire as the counter electrode and an Ag/AgCl as the reference electrode. The light was produced by using a solar simulator at 100 mW/cm^2 intensity. Electrochemical impedance spectroscopy (EIS) measurements were also performed on the same electrochemical workstation over a frequency range from 0.01 Hz to 100 kHz at the open-circuit voltage.

2.5 Photodegradation test

The photocatalytic activity of catalysts was evaluated by the degradation of Rhodamine B (RhB) in an aqueous solution. A general procedure was carried out as follows: First, 50 mL aqueous RB solution (1×10^{-5} mol/L) was placed in a reactor. Then, 20 mg catalyst was suspended in the solution. The suspension was stirred vigorously for 60 min in the dark to establish adsorption–desorption equilibrium of RhB. The suspension was then irradiated under visible-light. Samples were withdrawn periodically from the reactor, then centrifuged and analysed by recording variations in the absorption in the UV–vis spectra of RhB at its characteristic wavelength of 553 nm.

3. Results and discussion

The morphology and microstructure of as-prepared TiO_2-RGO nanocomposite was scrutinized by SEM. As shown in Figure 1A, the morphology of TiO_2 nanoparticles show a slight tendency to agglomerate. Meanwhile, the RGO sheets remain their thin sheet structure with no obvious re-stacking effect, indicating the introduction of TiO_2 nanoparticles between RGO sheets could effectively prevent the aggregation of GO after reduction process. The reduction of GO and formation of TiO_2 nanoparticles occurred simultaneously under ultrasonication. The TiO_2-RGO nanocomposites exhibited a homogeneous dispersion. The elemental information of the as-prepared nanocomposite was analyzed by EDX. As shown in Figure 1B, the EDX spectrum of TiO_2-RGO nanocomposite shows the only existence of C, O and Ti, indicating the successful formation of nanocomposite with high purity. The signal for C should mainly originate from the RGO sheets, while those for Ti are from the TiO_2 nanoparticles. The signal of O could contribute by TiO_2 nanoparticles and small amount of oxygen-containing groups on RGO sheets.

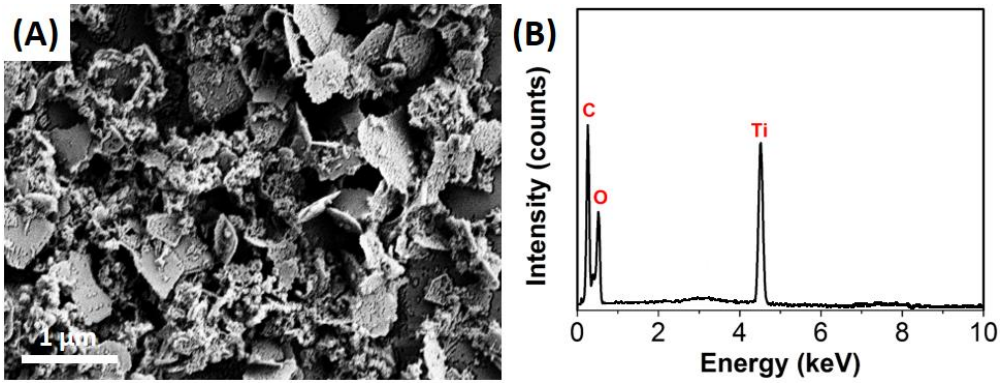

Fig. 1. SEM image and EXD spectra of TiO_2-RGO nanocomposite.

Raman spectra can be used to accurately determine the crystal structure of graphene after chemical treatment. Fig. 2A shows the Raman spectra of GO and TiO_2-RGO nanocomposite. As shown in figure, the Raman spectrum of GO contains D and G bands at 1344 and 1591 cm^{-1}, respectively. The D band and G band can be assign to the first-order scattering of E_{2g} phonons by sp^2 carbon atoms and breathing mode of κ-point photons of A_{1g} symmetry, respectively [24]. In the Raman spectrum of TiO_2-RGO nanocomposite, the D band is broadened and shifted to 1355 cm^{-1}

compared with that for GO. The G band also shifted to around 1602 cm^{-1}. The intensity ratio of the D and G peaks (I_D/I_G) increases from 0.826 to 0.971 for the TiO_2-RGO nanocomposite, indicating the restoration of sp^2 domains on reduction under ultrasonication condition.

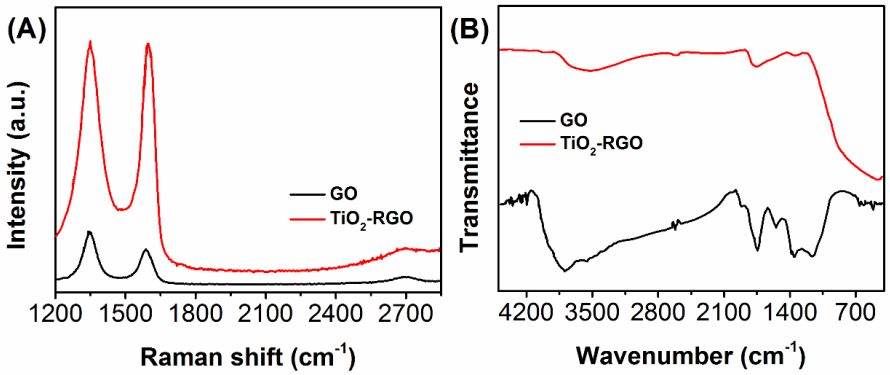

Fig. 2. (A) Raman and (B) FTIR spectra of GO and TiO_2-RGO nanocomposite.

FTIR analysis is used to analyse the reduction of GO and formation of TiO_2-RGO nanocomposite. Figure 2B shows FTIR spectra of the GO and the TiO_2-RGO nanocomposite. The spectrum of GO displays peaks at 1710, 1592, 1398 and 1024 cm^{-1}, which belong to the C═O stretching of COOH groups, C=C vibrations, C—OH stretching vibrations and C—O vibrations from alkoxy groups, respectively [25-27]. These peaks decreased dramatically in intensity or even disappeared after ultrasonication assisted reduction, suggesting the oxygen-containing functional groups in GO were decomposed. Moreover, the strong absorption around 450 cm^{-1} is attributed to the vibration of Ti–O–Ti bonds in TiO_2, indicating the formation of TiO_2-RGO nanocomposite.

The elemental information and the internal interaction were also investigated by XPS. Figure 3A shows XPS survey of the TiO_2-RGO nanocomposite, which presents the existence of Ti, O, and C with the chemical binding energies of $Ti2p_{3/2}$, O1s and C 1s, respectively. The investigation of carbon states (Figure 3B) shows the presence of two types of carbon bonds, that is, C–C (284.7 eV) and Ti-O–C (288.1 eV) [28]. The presence of the Ti–O–C structure revealed that the C atoms have substituted some of the Ti atoms in the TiO_2 lattice during the ultrasonication preparation.

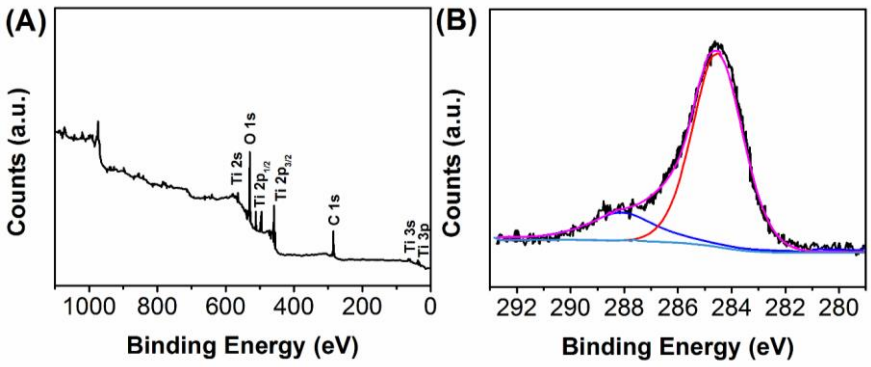

Fig. 3. (A) XPS survey spectrum and (B) C1s spectrum of the TiO_2-RGO nanocomposite.

Fig. 4A shows the XRD patterns of GO and TiO_2-RGO nanocomposite. The XRD pattern of GO displays a characteristic peak at 11.47° corresponds to the (001) reflection of graphite oxide, which indicates that most of the graphite power was oxidized into GO by expanding d-spacing from 3.2 Å to 6.64 Å [29, 30]. A series of characteristic peaks are noted in the XRD pattern at 2 θ of 25.1°, 37.5°, 47.9°, 54.2°, 55.0°, 63.2°, 69.3° and 70.1° for TiO_2-RGO nanocomposite, which

related to the (101), (004), (200), (105), (211), (118), (116) and (220) crystallographic plane of anatase, respectively. Moreover, the TiO_2-RGO nanocomposite did not shows a broad diffraction peak around 22°, indicating the TiO_2 nanoparticles effectively separated RGO sheets.

Photoluminescence (PL) spectroscopy can provide useful information about the efficiency of charge carrier trapping and recombination in semiconductor particles. Figure 4B presents the PL measurement for pure TiO_2 and TiO_2-RGO nanocomposite. As shown in the figure, both spectra show similar trends, which have strong peaks located at ca. 397 nm, responding to the emission of band gap transition with the energy of light approximately equal to the band gap energy of anatase [31]. Other peaks observed in the wavelength ranging from 430 to 520 nm are attributed to excitonic PL, which mainly result from surface oxygen vacancies and defects [32]. It can be observed that the PL intensity of TiO_2-RGO nanocomposite is much less than that of TiO_2 nanoparticles, indicating that the composite has a lower recombination rate of electrons and holes under light irradiation. This phenomena is ascribed to the fact that the electrons are excited from the valence band to the conduction band and then transferred to RGO sheets due to its excellent electronic conductivity, preventing a direct recombination of electrons and holes.

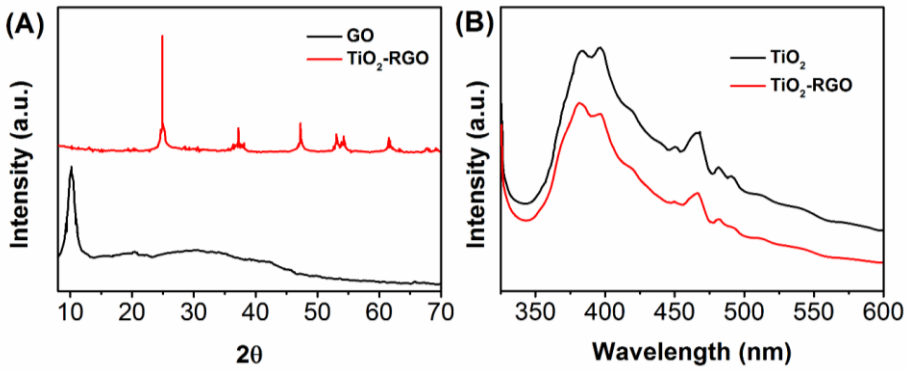

Fig. 4. (A) XRD patterns of GO and TiO_2-RGO nanocomposite. (B) Photoluminescence spectra of TiO_2 and TiO_2-RGO nanocomposite

Figure 5A shows the UV-vis diffuse reflectance spectra of the as-prepared TiO_2 and TiO_2-RGO nanocomposite. It can be observed that two spectra exhibit a characteristic absorption band around 400 nm, indicating the existence of highly crystallized TiO_2. Meanwhile, a red shift was observed in the TiO_2-RGO nanocomposite compared with that of TiO_2 nanoparticles, indicating a narrowing of the band gap of TiO_2. Moreover, The spectrum of TiO_2 has relatively lower absorption intensity in the visible region compared with TiO_2-RGO nanocomposite. A plot of the transformed KubelkaMunk function as a function of energy of light is shown in Figure 5B. The band gap of TiO_2, and TiO_2-RGO nanocomposite has been determined as 3.31 and 2.88 eV, respectively. This supports the qualitative observation of a red shift in the absorption edge.

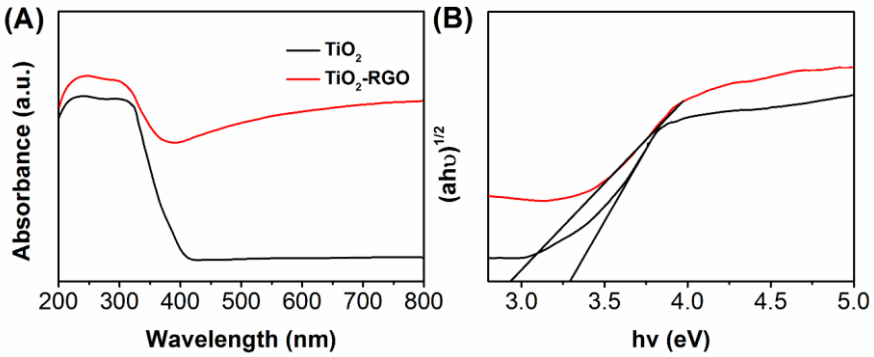

Fig. 5. (A) UV-vis diffuse reflectance spectra (DRS) and (B) the plot of transformed KubelkaMunk function versus the energy of light of TiO_2 and TiO_2-RGO nanocomposite

The photocatalytic activities for the TiO_2-RGO nanocomposite was measured by the degradation of Rh B under UV–vis light irradiation. P25 and pure TiO_2 nanoparticles were used as control groups. As shown in Figure 6A, the Rh B shows a tiny self-degradation process after 180 min irradiation. The photodegradation rates of bare P25 and pure TiO_2 are 328% and 70% after 180 min irradiation, respectively. In contrast, the TiO_2-RGO nanocomposite exhibits a prominent performance, which can degrade more than 98 % of Rh B in 180 min. The apparent rate constant of TiO_2-RGO nanocomposite (0.02432/min) was found to be almost 2-fold than that of TiO_2 nanoparticles (0.01166/min) and 12-fold than P25 (0.00223/min), which implies the introduction of RGO into TiO_2 nanoparticles could highly enhance the photodegradation rate.

The stability of photocatalyst during photocatalytic reaction is a crucial consideration in the practical applications. Thus, the reusability test of the synthesized photocatalyst was carried out using TiO_2-RGO nanocomposite for 7 photodegradation cycles. As shown in Figure 6B, the TiO_2-RGO nanocomposite could remain more than 85% of photocatalytic performance after 7 cycles photodegradation, implying that the proposed nanocomposite has excellent stability. The slight decreasing performance might due to the photocatalysts loss during the washing process after each photodegradation cycle and surface retardant by organic intermediates.

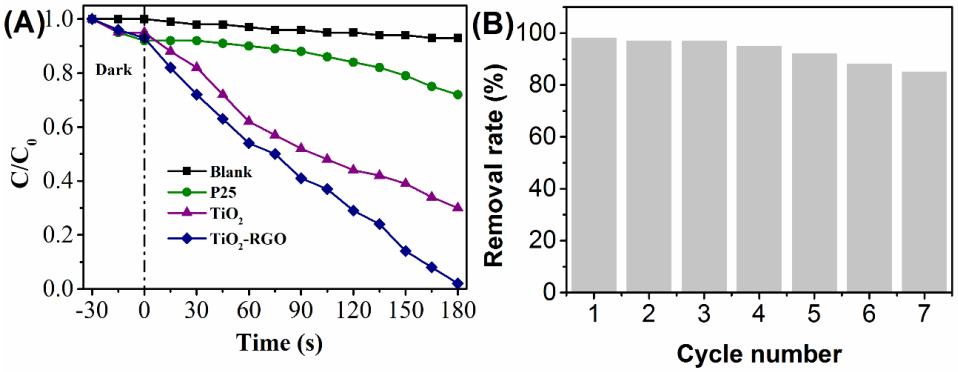

Fig. 6. (A) Photodegradation profiles of Rh B using various photocatalyst under visible light illumination. (B) The stability test of TiO_2-RGO nanocomposite.

The photoelectrochemical properties of TiO_2-RGO nanocomposite was investigated by a series of photoelectrochemical experiments. Figure 7A shows the photocurrent densities of TiO_2 and TiO_2-RGO nanocomposite under visible illumination. As expected, the TiO_2-RGO nanocomposite showed a significant photocurrent response compared with that of pure TiO_2. The higher photocurrent density of TiO_2-RGO nanocomposite was indicative of an improved optical absorption capability and an enhanced separation of photogenerated electrons and holes as compared to pure TiO_2. Figure 7B shows the typical current density–voltage (J–V) curves of TiO_2 and TiO_2-RGO nanocomposite during illumination. It can be seen that the short circuit current density (JSC) and conversion efficiency (h) of pure TiO_2 were very low, which are 0.101 mA/cm^2 and 0.013%, respectively. In contrast, the η of TiO_2-RGO nanocomposite was 0.142% with a JSC of 1.119 mA/cm^2. This was consistent with the results of the photocurrent response, suggesting that incorporation of RGO can act as an electron acceptor to effectively improve the photovoltaic performance of the TiO_2 photocathode. Figure 7C shows the EIS measurements on TiO_2-RGO nanocomposite and pure TiO_2 at a potential of ─3.0 mV over the frequency range from 100 kHz to 0.01 Hz. Clearly, both impedance curves showed a semicircle in the intermediate frequency region. Moreover, the semicircle diameter of TiO_2-RGO nanocomposite is much smaller than that of pure TiO_2, suggesting that the TiO_2-RGO nanocomposite possessed a lower charge transfer resistance, thereby leading to the increased photocurrent conversion efficiency.

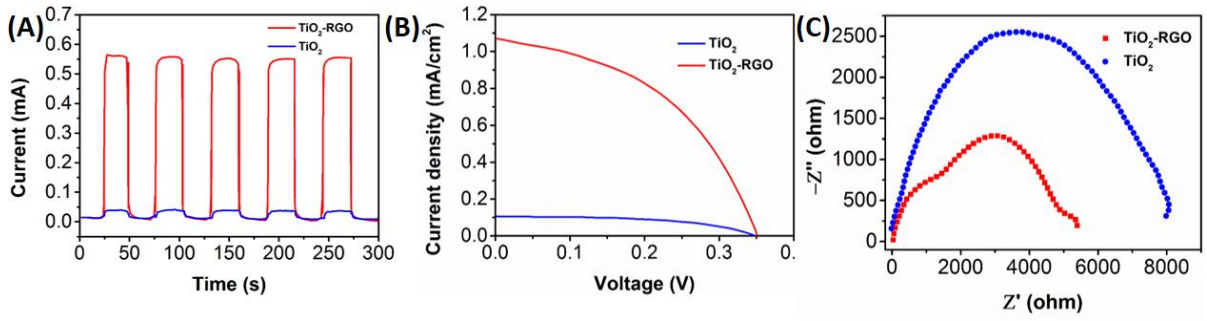

Fig. 7. (A) Photo-current responses, (B) current density–voltage characteristics and (C) electrochemical impedance spectra of TiO_2 and TiO_2-RGO nanocomposite

4. Conclusion

In summary, the incorporation of TiO_2 with RGO sheets and for high efficient photocatalytic and photovoltaic applications was systematically researched. The TiO_2-RGO nanocomposites were synthesized by a simple ultrasonication method. As confirmed by the characterizations, the incorporation of RGO and Pd with TiO_2 could facilitate the electron transfer, light absorption and electrical conductivity of photocatalyst. As a result, the TiO_2-RGO nanocomposite showed a significant enhancement in photodegradation of Rh B and. Photovoltaic performance.

Reference

[1] L. Fu, Y.-H. Zheng, Z.-X. Fu, Chemical Papers **69,** 655 (2015).
[2] Z. Ji, R. Wu, L. Adamska, K.A. Velizhanin, S.K. Doorn, M. Sykora, ACS applied materials & interfaces **6,** 20473 (2014).
[3] H.U. Hanif, M. Arshad, M.A. Ali, N. Ahmed, I.A. Qazi, Pak. J. Agri. Sci **52,** 177 (2015).
[4] M.R.d. Souza, N.T. Oliveira, N.K. Kuromoto, C.E. Marino, Matéria (Rio de Janeiro) **19,** 53 (2014).
[5] D. Fakin, K.S. Kleinschek, A. Ojstr²ek, Acta Physica Polonica A **127,** 943 (2015).
[6] C. Wang, W. Zhang, H. Huang, J. Wu, Y. Gan, X. Tao, Asian Journal of Chemistry **26,** (2014).
[7] L. Zhu, S.-B. Jo, J.-H. Jo, S. Ye, K. Ullah, W.-C. Oh, Journal of the Korean Ceramic Society **51,** 139 (2014).
[8] L. Zhang, C. Ma, J. Wang, S. Li, Y. Li, B. Wang, Russian Journal of Physical Chemistry A **88,** 2435 (2014).
[9] G. Mamba, X. Mbianda, A. Mishra, Environmental Science and Pollution Research **21,** 5597 (2014).
[10] N.M. Mahmoodi, Water, Air, & Soil Pollution **224,** 1 (2013).
[11] F. Zhang, F. Xie, H. Xu, J. Liu, W.C. Oh, Kinetics and Catalysis **54,** 297 (2013).
[12] L. Fu, A. Yu, Rev. Adv. Mater. Sci **36,** 40 (2014).
[13] L. Fu, A. Yu, Carbon nanotube based nanostructured thin films: preparation and application, Fourth International Conference on Smart Materials and Nanotechnology in Engineering, International Society for Optics and Photonics, 2013, pp. 87930T.
[14] D. Zhang, Y. Gao, X. Pu, W. Li, C. Su, P. Cai, H.J. Seo, Science of Advanced Materials **6,** 2632 (2014).
[15] Y.-q. Zhang, X.-h. Li, J. Lü, C.-d. Si, G.-j. Liu, H.-t. Gao, P.-b. Wang, International Journal of Minerals, Metallurgy, and Materials **21,** 813 (2014).
[16] M. Aleksandrzak, M. Onyszko, B. Zielińska, E. Mijowska, International Journal of Materials Research **105,** 900 (2014).
[17] Z. Cheng, D. Ding, X. Nie, Y. Xu, Z. Song, T. Fu, Z. Chen, W. Tan, Science China

Chemistry 1 (2015).
[18] Z. Yao, M. Wang, S. Sun, R. Jia, H. Li, Journal of Inorganic and Organometallic Polymers and Materials **24,** 315 (2014).
[19] C. W Lai, F. W Low, S. W Chong, C. PP Wong, B.M. Siddick, Z. Siti, J. C Juan, S. B Abdul Hamid, Current Organic Chemistry **19,** 1882 (2015).
[20] X. Wang, X. Liu, X. Xue, H. Pan, M. Zhang, Q. Li, L. Yu, J. Yang, Z. Zhang, Journal of nanoparticle research **15,** 1 (2013).
[21] G. Williams, B. Seger, P.V. Kamat, ACS Nano **2,** 1487 (2008).
[22] W. Fan, Q. Lai, Q. Zhang, Y. Wang, J Phys Chem C **115,** 10694 (2011).
[23] W.S. Hummers, R.E. Offeman, Journal of the American Chemical Society **80,** 1339 (1958).
[24] Z.-J. Fan, W. Kai, J. Yan, T. Wei, L.-J. Zhi, J. Feng, Y.-m. Ren, L.-P. Song, F. Wei, ACS Nano **5,** 191 (2010).
[25] J. Zhang, H. Yang, G. Shen, P. Cheng, J. Zhang, S. Guo, Chemical Communications **46,** 1112 (2010).
[26] M. Ahmad, E. Ahmed, Z.L. Hong, J.F. Xu, N.R. Khalid, A. Elhissi, W. Ahmed, Appl. Surf. Sci. **274,** 273 (2013).
[27] X. Li, Q. Wang, Y. Zhao, W. Wu, J. Chen, H. Meng, Journal of colloid and interface science **411,** 69 (2013).
[28] Q. Bao, S. Bao, C.M. Li, X. Qi, C. Pan, J. Zang, Z. Lu, Y. Li, D.Y. Tang, S. Zhang, K. Lian, J Phys Chem C **112,** 3612 (2008).
[29] T. Nakajima, A. Mabuchi, R. Hagiwara, Carbon **26,** 357 (1988).
[30] A.B. Bourlinos, D. Gournis, D. Petridis, T. Szabó, A. Szeri, I. Dékány, Langmuir **19,** 6050 (2003).
[31] J. Yu, T. Ma, G. Liu, B. Cheng, Dalton Transactions **40,** 6635 (2011).
[32] J. Yu, T. Ma, S. Liu, Phys Chem Chem Phys **13,** 3491 (2011).